Characterization of the Structural Response of Adhesively Bonded Ultra-High Strength Steel Tubes under a Range of Loading Conditions and Assessment of a Rate Dependent Cohesive Zone Model

Brian Liu[1], Brock Watson[1], Michael Worswick[1], Duane Cronin[1]

[1] Department of MME, University of Waterloo, 200 University Avenue West, Waterloo, Canada

Submitted to: Journal of Dynamic Behavior of Materials

Corresponding Author: Prof. Duane Cronin
Department of Mechanical Engineering
University of Waterloo
200 University Ave. West
Waterloo, Ontario, Canada, N2L 3G1
dscronin@uwaterloo.ca
(519) 888-4567 x32682

Declarations of conflict of interest: none

Word Count: 6,682 (Introduction to Conclusions)

Abstract

Weight reduction through the use of adhesive joining in multi-material lightweight structures requires material characterization and substructure level model validation to support CAE design. In this study, automotive-scale structural tubes were created by adhesively joining tailored hot stamped (THS) ultra-high strength steel (UHSS) hat sections using a two-part toughened epoxy adhesive applied to the flanges. A custom fixturing method was developed to achieve consistent bond line thickness for the adhesive joint. The physical tubes were tested in three-point bend, axial crush, and Mode I loading at quasi-static and dynamic loading rates, from which the structural response and failure characteristics were established.

The experiments were modeled numerically using a previously developed cohesive zone method (CZM) that had been validated for coupon level tests. In the current work, the CZM model is assessed under structural loading conditions, based on predictions of load-displacement response, peak load, energy absorption, displacement-to-failure, and deformation pattern. In addition, crack extension along the adhesive joint was assessed for the Mode I loading condition. The novel bonding procedure developed for this study resulted in consistent experimental loading response. Generally, the predicted results agreed with experimental results, particularly for the Mode I loading and crack extension behavior. However, the CZM model was not able to accurately predict displacement-to-failure for the three-point bend tests, owing to out-of-plane buckling observed in the experiments. With a few exceptions, the CZM adhesive model based on coupon-level data was able to predict the peak force, displacement-to-failure, and energy absorption of the bonded structural assemblies to within 16% of the average experimental responses.

Keywords: structural adhesive, cohesive zone model, tailored hot stamping, ultra-high strength steel, impact testing

1. Introduction and Background

The need for vehicle weight reduction to improve fuel economy and reduce emissions has led to the pursuit of multi-material lightweight vehicle (MMLV) designs using advanced high strength steels, lightweight alloys, and composites [1]; however, joining of dissimilar materials presents challenges for many traditional joining processes. Structural adhesives are a promising alternative to traditional welding or mechanical connections and can be used to address some of the challenges of dissimilar material joining [2]. For example, adhesive joints can act as a physical barrier between dissimilar materials to prevent galvanic corrosion, reduce stress concentrations by increasing stress-bearing area, and improve NVH performance by increasing joint stiffness [3]. These structural benefits, as well as the introduction of a sealed joint, have led to increased usage of adhesive joining in automotive structures [4]. However, the ability to efficiently and accurately model adhesive joints to predict their mechanical behavior in crash scenarios is a critical requirement for adhesives to become more widely adopted in vehicle design [4, 5].

Hot stamped ultra-high strength steels (UHSSs) [6] are widely used in vehicle structures with more recent developments including in-die heating to tailor hot stamped (THS) material properties within a part for optimization of crash performance [7]. In THS, cooled regions of the tooling subject the part to a higher cooling rate to produce a hard, ultra-high strength martensitic microstructure, while heated regions with a slower cooling rate can produce a softer, more ductile bainitic/ferritic microstructure [8]. Advancements in THS have led to the development of automotive structures with a strategic combination of hardened areas for intrusion resistance and softened areas for energy absorption [9, 10].

Similarly, many researchers have investigated the experimental testing and numerical modelling of adhesively bonded structures under various loading conditions [11,15-19]. Gowda *et al.* [20] investigated dynamic three-point bending of double-hat section tubes joined by spot welding, adhesive bonding, and a combination of the two. While registered peak loads were comparable, the bonded tubes experienced complete separation of the flange, which rapidly reduced the transverse load bearing capability. Lee *et al.* [21] compared the crash performance of adhesively bonded and self-pierce riveted (SPR) steel-aluminum tubes against spot-welded steel-steel (cold-rolled) tubes under dynamic axial crush. The tubes were found to have considerably higher specific energy absorption, with that of the adhesive bonded tubes being slightly lower than that using SPRs. Peroni, Avalle, and Belingardi [22] conducted an extensive study comparing the energy absorption capability of steel crush tubes assembled by spot welding and continuous joining methods (laser welding and adhesive bonding) under static and dynamic axial loading. A key finding of this study was that the energy absorption capability of bonded tubes was heavily dependent on countermeasures to avoid rapid debonding of the adhesive joint. In a subsequent study, Avalle *et al.* [23] used the cohesive zone modelling (CZM) approach to predict the response of bonded crush tubes under static axial loading with less than 10% deviation from experimental data based on average load. A similar conclusion was drawn in a study by Trimiño and Cronin [24], in which the applicability of the non-direct similitude (NDS) technique to model bonded structures was investigated. The measured response from sub-scaled tubes tested in dynamic axial impact loading was used to assess the predictive capabilities of scaled up numerical models. A major outcome of this study was that CZM elements provided a good representation of adhesive joints. While experimental and numerical studies of bonded structures are abundant in

70 the literature, few have explored the adhesive joining of full scale UHSS structures, particularly
71 those fabricated using tailored hot stamped components, which display a wide range of material
72 properties and deformation within a single component.

73 While many modelling methodologies have been developed, common numerical representations
74 of the adhesive joint include tiebreak contacts, cohesive elements (CZM), and continuum solid
75 elements [25, 26]. Tiebreak contacts are efficient and simple implementations but are susceptible
76 to numerical instabilities (unzipping), while an adhesive joint represented by a large number of
77 solid elements can be accurate but may be computationally prohibitive [26]. The CZM method is
78 a more comprehensive approach than a tiebreak contact for modelling fracture behavior in
79 adhesive joints [27] and has been shown to be accurate yet computationally efficient compared
80 to solid element models of the adhesive [26]. With CZM, the adhesive bond line is represented
81 by defining a single row of elements between the adherends. CZM uses both strength and energy
82 parameters to characterize the fracture process, whereby damage is assumed to accumulate
83 ahead of an extending crack tip, eventually leading to failure that follows a pre-defined path [25].
84 As such, the material response of adhesive joints represented with CZM is described by the
85 traction-separation (stress-displacement) curves in the normal (Mode I) and shear (Mode II)
86 directions [28]. Traction-separation curves can be represented with different shapes, with the
87 trapezoidal shape being more suited for ductile adhesives [29]. The trapezoidal law is defined by
88 several parameters including the undamaged material stiffness, peak traction, critical energy
89 release rate, and ratio of plastic deformation relative to total deformation [4].

90 The current study examines the application of CZM techniques to simulate the behaviour of
91 adhesively-bonded structural components, of size and forming history comparable to those used

92 in contemporary automotive structures. Of particular interest is the application to ultra-high
93 strength hot stamped structural components, in this case considering Usibor ®1500-AS, since very
94 little previous work has examined adhesive bonding of such components. Tailored hot stamped
95 components are also examined since such their impact response involves both ultra high stress
96 (in intrusion-resistant zones) and high deformation (in energy-absorption zones). THS double-hat
97 sections were fabricated and were adhesively joined to form tubes. Three different loading
98 modes were considered: three-point bend, axial crush and Caiman (Mode I) loading. Both static
99 and dynamic loading were considered for each loading case. Numerical models of the
100 experiments were developed using published material data from Watson *et al.* [30]. The ability
101 of the CZM model to predict the crash response of bonded full-scale structures was quantitatively
102 assessed.

2. Experimental Methodology

Hat sections representing automotive structural members were tailor hot stamped with various tailoring configurations, adhesively bonded to form a double hat-section, and tested in three loading conditions: three-point bend (3P), axial crush (AX), and the Mode I Caiman (CM) fracture tests (Figure 1).

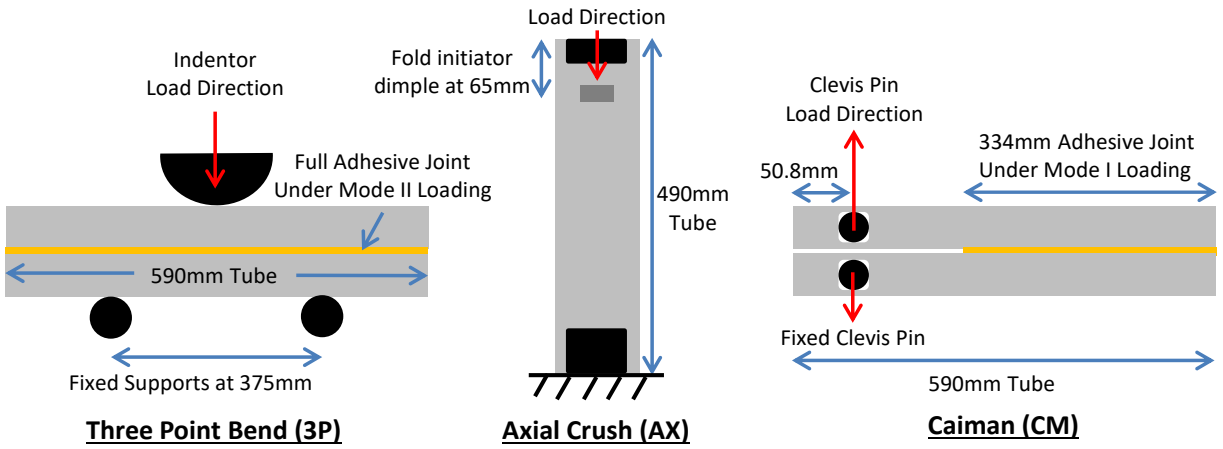

Figure 1: Schematic of the three loading conditions (3P, AX, CM) showing load points (black), adhesive (yellow), and steel (grey). Dimensions indicated with blue arrows, applied loads indicated with red arrows.

2.1 Tailored Hot Stamping Process

The hat sections were hot stamped using 1.2 mm Usibor® 1500-AS sheet using three configurations (Figure 2). The first configuration comprised fully martensitic (FM) specimens, that were fully quenched (no tailoring) during forming. In the second configuration, soft flange (SF) specimens were produced with the tooling adjacent to the flanges heated to 600 °C while the balance of the tool was cooled, resulting in lower hardness and lower strength flanges. The third configuration, used for axial crush testing, considered "three zone" (3Z) specimens by

preferentially heating the tooling adjacent to the flanges as well as the center of the hat section to 400 °C, while the tooling at the impacted end of the hat section was heated to 700 °C. Details of the hot stamping process are given by Prajogo [12] for the SF configurations and by Omer *et al.* [13] for the 3Z configuration. A blank size of 220 x 590 mm was used, which resulted in flange widths that were amenable to adhesive bonding.

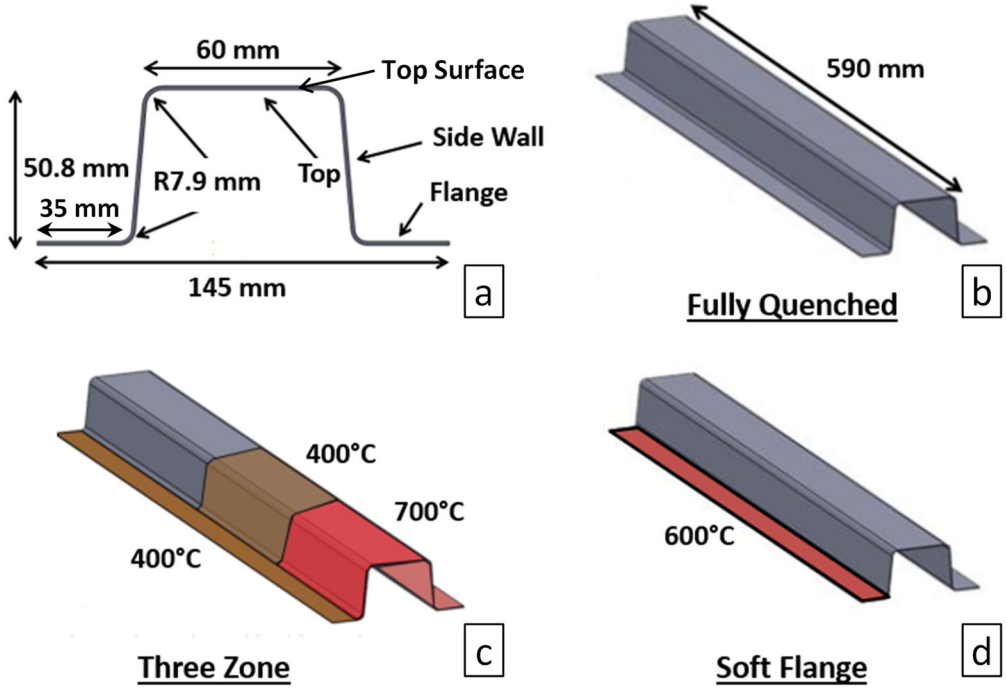

Figure 2: Hat section a) cross-section dimensions, b) length dimensions and fully martensitic hat section (grey), c) three-zone (3Z) hot stamping configuration, and d) soft flange (SF) hot stamping configuration. Figures b) and c) from Omer et al. [13]. Figure d) from Prajogo [12].

To verify that the desired tailoring configurations were achieved, micro-hardness measurements (Wilson Hardness VICKERS 402 MVD) were taken on the flange, side wall, and top surface for each of the three tailoring configuration hat sections. A load of 1000 g and a pyramidal indenter were used to measure the Vickers Hardness. Three specimens were extracted from each of two

randomly selected hat sections for testing the FM and SF conditions, while five sections were cut from each of three randomly selected hat sections for the 3Z condition to confirm the progressive change in hardness for this tailoring condition.

A fold initiator (see axial crush schematic in Figure 1) was formed in the hat sections used for the axial crush specimens after hot stamping and prior to bonding. The initiator comprised a 4 mm deep dimple that was formed 65 mm from the impacted end of the section using a punch measuring 25 mm x 10 mm with a 5 mm fillet radius on all its edges. A manual hydraulic press was used to form the fold initiator, which served to initiate a progressive folding deformation during the axial crush experiments. The length of all axial crush specimens was also reduced from 590 mm to 490 mm to reduce the likelihood of column buckling.

2.2 Adhesive Joining of Hat Sections

The adhesive used to join the hat sections was a toughened epoxy structural adhesive (IRSA 07333, 3M, Minnesota). A nominal bond line thickness of 0.178 mm (0.007”) was targeted for all specimens, as per the manufacturer’s specifications. The adherend surfaces were prepared to improve joint strength and reduce variability in order to achieve consistent cohesive failure in the adhesive joint. Following the procedure outlined by Liao *et al.* [31], all bond surfaces on the hat sections were grit blasted with 60 grit aluminum oxide to remove the intermetallic Al-Si layer on the hot stamped metal surface. Subsequently, circular shims were evenly distributed along the flange and kept in place with a fast-acting ethyl cyanoacrylate adhesive [32] to maintain a uniform bond line thickness (Figure 3a). Acetone was used to clean the flange surface

immediately prior bonding. The structural adhesive was applied to both sides of the flanges and spread into a thin uniform layer with a spatula while avoiding the shims. The hat sections were then clamped together by aligning c-clamps acting on the circular shim locations and securing 12.5 mm (0.5”) steel bars over the flanges (Figure 3b). Any excess adhesive that was squeezed out of the flanges was removed. The assembly was cured in a forced convection oven at 80 °C for 30 minutes.

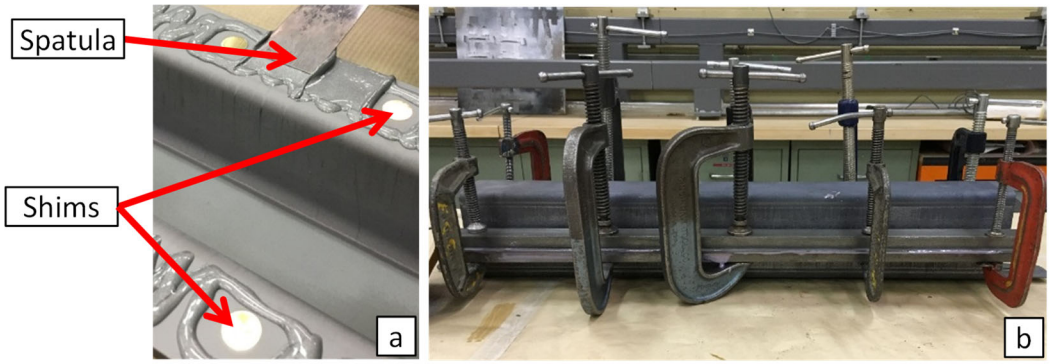

Figure 3: a) Spreading adhesive with a spatula, with circular brass shims to maintain bond line thickness during curing, and b) hat section clamping fixture.

2.3 Experimental Testing of Bonded Hat Sections

The experimental testing comprised a total of 10 conditions (Table 1) including loading rate, load condition (3P, AX, CM) and three different hot stamp tailoring conditions. Three repeats were conducted for each test.

Table 1: Summary of test conditions and designation for loading rate, loading condition, and hot stamping condition.

Load Rate	Load Condition	Tailoring	Repeats	Designation
Quasi-Static	3 Point Bend	Fully Martensitic	3	QS-3P-FM
Quasi-Static	3 Point Bend	Soft Flange	3	QS-3P-SF
Dynamic	3 Point Bend	Fully Martensitic	3	DM-3P-FM
Dynamic	3 Point Bend	Soft Flange	3	DM-3P-SF
Quasi-Static	Axial Crush	Fully Martensitic	3	QS-AX-FM
Quasi-Static	Axial Crush	3 Zone	3	QS-AX-3Z
Dynamic	Axial Crush	Fully Martensitic	3	DM-AX-FM
Dynamic	Axial Crush	3 Zone	3	DM-AX-3Z
Quasi-Static	Caiman	Fully Martensitic	3	QS-CM-FM
Quasi-Static	Caiman	Soft Flange	3	QS-CM-SF

A 496 kN hydraulic load frame with a crosshead velocity of 1.0 mm/s was used for the quasi-static three-point bend experiments. A 100 mm diameter indenter was mounted to the end of the piston and the tube rested on two 50 mm diameter cylindrical supports spaced 375 mm apart. To allow the tube to deform freely without binding to the tooling, the tooling surfaces were lined with two layers of Teflon film and a thin layer of petroleum jelly-based lubricant. Force and crosshead displacement were recorded at 4 Hz using a cylinder mounted load cell and LVDT respectively.

A 623 kN hydraulic load frame was used for the quasi-static axial crush experiments, with a crosshead velocity of 0.5 mm/s. The top of the crush tube was placed in fixture mounted to the end of the hydraulic piston, while the bottom of the tube was placed in a fixture mounted on the base plate of the load frame.

The Caiman experiments [14] were conducted using a 100 kN tensile load frame (MTS Criterion Model 45). The tensile frame pulled the unbonded end of the Caiman specimens apart, inducing

progressive cracking of the adhesive joint due to Mode I (peel) failure of the adhesive. The fixture utilized inner and outer bosses that clamped each half of the tube, and load was transferred from the clevises to the inner bosses through 19.05 mm diameter pins. Experimental images were continuously captured by two digital cameras (Point Grey Research GRAS-50S5M-C 5.0 MP) at 5 fps that were synchronized with the measured force and crosshead displacement data *via* commercial software (VIC SNAP 2009, Correlated Solutions). Further description of the Caiman test methodology and fabrication details are given by Tolton *et al.* [14].

An impact sled (Seattle Safety D780-3.7) [39] was used for dynamic three-point bend and axial crush experiments. The three-point bend experiments used the same fixtures as the quasi-static tests, but mounted horizontally on the reaction wall (Figure 4a). The indenter was mounted to a pack of two load cells (120 kN Kistler Quartz Force Link, model#9371B) attached to the impact sled, with a 19.05 mm thick wooden plate between them acting as a damper to reduce signal noise. The impact velocity for all dynamic three-point bend tests was 7.5 m/s and the total mass of the sled was 870 kg, similar to the experiments carried out by Projogo [12]. After an initial undisturbed deformation zone of 55 mm for the specimens, the impact sled made contact and was arrested by Plascore 5052 honeycomb. Two accelerometers were mounted in the back of the impact sled, and the sampling rate used for all load cells and accelerometers was 10,000 Hz, with no software filtering applied to the final data. Displacement was obtained by double-integrating the deceleration data from the accelerometers. The impact experiments were recorded with two high-speed digital cameras (Photron SA4/5) at 5000 fps.

The impact sled, accelerometers and high-speed imaging were also used in the dynamic axial crush experiments (Figure 4b). The mounting fixtures were also the same as those used in the

quasi-static axial crush experiments. The fixture base plate was mounted on three 120 kN Kistler load cells that were attached to the reaction wall in a triangular pattern. For the axial crush tests, the sled was configured with a total mass of 900 kg and a nominal impact velocity of 10 m/s, similar to the methods described by Omer et al. [13]. The specimens were allowed a free crush length of 145 mm before the sled was arrested by honeycomb packs.

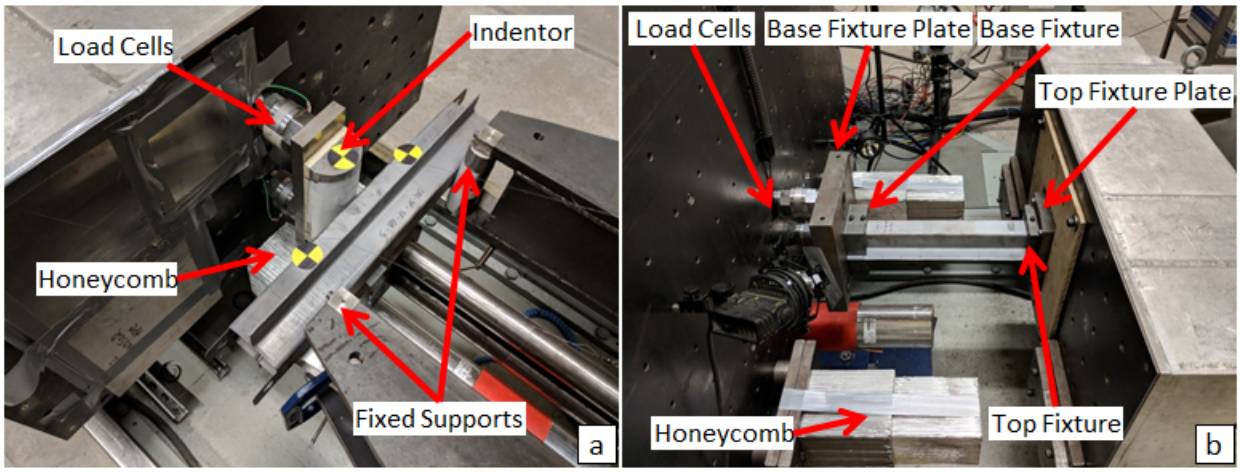

Figure 4: a) Dynamic experimental setup for three-point bend, b) and axial crush loading conditions.

3. Numerical Models of Adhesively Joined Test Specimens

Finite element simulations of the three load cases were developed using a commercial meshing software (Hypermesh, Altair) and solved using a commercial explicit finite element (FE) code (LS-DYNA R7.1.2, LST). Two channel hat parts were meshed and these were joined using CZM elements positioned between the two flanges. To account for the material properties resulting from the hot stamping process, the mechanical properties were mapped onto the hat section mesh based on material hardness distributions.

3.1 Finite Element Mesh of Hat Sections and Joining with CZM Elements

The finite element meshes used to model the three experiments are shown in Figure 5. Fully integrated shell elements (element type 16 in LS-DYNA) with a nominal element size of 2.5 mm and seven integration points through thickness (1.2 mm) were used to mesh the hat sections. The fold initiator was added to the axial crush tube models by translating a row of nodes 4 mm inwards at 65 mm from the top end of the hat section. Although this simplified approach did not consider local work hardening and thinning, the created initiator was sufficient in terms of initiating folding.

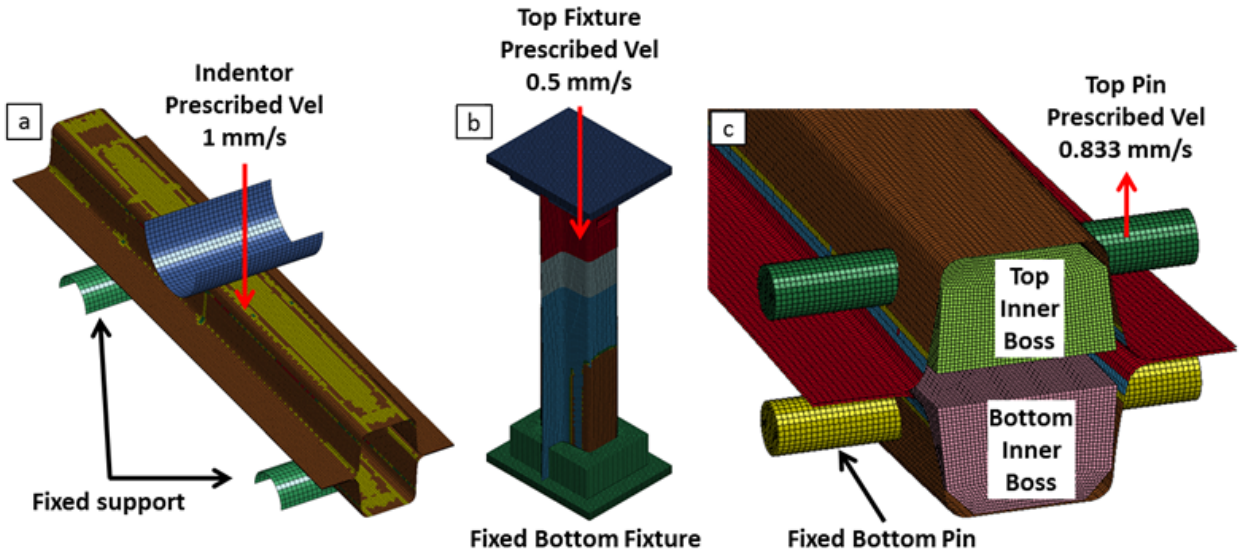

Bin	FM Vickers Hardness Range (Weighted Average)
1	456 – 462 (459.4)
2	463 – 468 (465.5)
3	469 – 474 (471.6)
4	475 – 480 (477.6)
5	481 – 487 (483.7)

Bin	3Z Vickers Hardness Range (Weighted Average)
1	187 – 248 (209.0)
1.5	(~240)
2	249 – 309 (270.1)
3	310 – 372 (331.1)
4	373 – 433 (392.4)
5	434 – 493 (473.5)

Bin	SF Weighted Average Vickers Hardness
1	254.1
2	301.4
3	358.3
4	424.2
5	486.2

Figure 5: Quasi-static model setup for a) three-point bend with FM hat section hardness distribution, b) axial crush with 3Z hardness distribution, c) and the Caiman with SF hardness distribution.

A single layer of cohesive elements was created between the hat section flanges to represent the adhesive joint, with a thickness of 0.178 mm (0.007”). A 0.6 mm gap between the surface of the CZM elements and the flange shell elements was used to account for the shell element thickness since the shell elements were meshed at the thickness mid-plane. An eight-node (4 integration point) cohesive element formulation [30] was assigned to the cohesive elements.

3.2 Material Model for Hot Stamped Channel Section

In order to illustrate the hardness distributions assigned in the models, the three-point bending model (Figure 5a) shows contours corresponding to the hardness distribution for a fully

martensitic hat section from [13]. The axial crush model (Figure 5b) shows contours corresponding to the 3Z hardness measurements performed as part of the current research. Finally, plot of the Caiman model (Figure 5c) shows contours of hardness based on [12] for the same soft flange tailored condition.

The material properties of the elements within each hat section were assigned according to the respective hardness map for each tailoring case. In order to limit the number of discrete material property sets, the elements within each hat section model were sorted into five equally divided bins within the full hardness range, following the approach developed by George *et al.* [6]. Rate-sensitive constitutive properties corresponding to the average hardness of each bin were then assigned based on the constitutive modelling work of Bardelcik *et al.* [33] which invokes a von Mises yield criterion and a piecewise linear hardening response. In addition, fracture of the fully martensitic hat section was modelled using the Generalized Incremental Stress-Strain Model (GISSMO) [34, 35] with the fracture *locus* developed by Samadian [36] for Usibor® 1500-AS. Fracture was not considered in the tailored conditions since this was not observed in the experiments (i.e. only the adhesive layer exhibited failure in the actual experiments).

3.3 Structural Adhesive Material Model

The CZM material model parameters measured and validated by Watson *et al.* [30] for the structural adhesive used in this study (Table 2) were implemented using a trapezoidal traction-separation response [18] for both quasi-static (QS) and dynamic (DM) load rates. The CZM parameters were based on Mode I properties measured using the rigid double cantilever beam

methodology [30], while the Mode II parameters were measured using a bonded shear sample [37]. To accommodate the gap created by the offset between the flange shell element reference plane and the adhesive layer (corresponding to one-half of the sheet metal thickness or 0.6 mm), a penalty-based tied constraint was defined, which allowed for moment transfer between the flange and adhesive layer. This methodology has been demonstrated to accurately model the response of adhesive joints at the coupon level [38].

Table 2: CZM material parameters for IRSA 7333 structural adhesive used in the adhesive model for quasi-static (QS) and dynamic (DM) simulations [30, 37].

Adhesive CZM Model Parameters	QS Value	DM Value
Density (ρ) [kg/m^3]	1200	-
Mode I Initial Stiffness (E) [MPa/mm]	1560	3166
Mode II Initial Stiffness (G) [MPa/mm]	1301	2333
Mode I Critical Energy Release Rate ($G_{IC,0}$) [N/mm]	3.055	0.004993
Mode I Critical Energy Release Rate ($G_{IC,\infty}$)	-	3.234
Mode II Critical Energy Release Rate ($G_{IIC,0}$)	6.345	0.1241
Mode II Critical Energy Release Rate ($G_{IIC,\infty}$)	-	7.337
Equivalent Strain Rate at Yield Initiation ($\dot{\varepsilon}_{GIC}$) [s^{-1}]	-	3.032e-04
Equivalent Strain Rate at Yield Initiation ($\dot{\varepsilon}_{GIIC}$) [s^{-1}]	-	0.01406
Mode I Yield Stress (T0) [MPa]	39.97	36.97
Mode I Yield Stress (T1) [MPa]	-	3.481
Mode II Yield Stress (S0) [MPa]	28.54	24.05
Mode II Yield Stress (S1) [MPa]	-	1.423
Equivalent Strain Rate at Yield Initiation ($\dot{\varepsilon}_T$) [s^{-1}]	-	5.363e-04
Equivalent Strain Rate at Yield Initiation ($\dot{\varepsilon}_S$) [s^{-1}]	-	5.570e-04
Mode I Ratio of Plastic to Total Area (FG1) [-]	0.1312	0.4133
Mode II Ratio of Plastic to Total Area (FG2) [-]	0.9000	0.9000

3.4 FE Model Boundary Conditions, Contact and Loading

In the three-point bend simulations (Figure 5a), the indenter and support surfaces were discretized using 2.5 mm rigid shell elements. The supports were constrained in all degrees of motion. The indenter was fixed in all degrees of freedom, except for the y-axis (loading direction), which was assigned a constant prescribed velocity of 1 mm/s for the quasi-static simulation. The dynamic three-point bend model used the same indenter, which was assigned a mass of 870 kg, corresponding to the mass of the sled, load cells and indenter assembly, and an initial velocity of 7.5 m/s, corresponding to the experimental conditions.

The fixtures in the axial crush models (internal bosses and external clamps, Figure 5b) were meshed using 2.5 mm rigid shell elements. In the static axial crush model, a prescribed velocity of 0.5 mm/s was used, while the dynamic model employed an impact mass of 900 kg and initial velocity of 10 m/s, corresponding to the experimental conditions.

The honeycomb crush arrestors used in the experiment to arrest the sled were not modelled, so only the impact response of each model within the free crush displacement (55 mm for three-point bend, 145 mm for axial crush) was compared to the experiment.

For the Caiman simulations (Figure 5c), both the pins and inner bosses were modeled as rigid bodies. The outer clamps were omitted as a simplification. The hat section nodes confined by the fixtures were constrained to the inner boss to simulate clamping. The bottom pin was fixed in all directions and the top pin was allowed translation only in the y-axis (vertical) with a prescribed velocity of 0.833 mm/s, while both inner bosses were free in all degrees of motion. Dynamic Caiman experiments were not considered in the current work.

297 In each simulation a penalty function-based contact was defined between all model parts with a
298 coefficient of friction of 0.4 [13]. The elastic properties of steel were assigned for use in the
299 penalty function stiffness calculation.

300 An explicit dynamic formulation was used for all simulations. Selective mass scaling was used in
301 the quasi-static simulations to achieve reasonable run times (about 40 hours) with a time step of
302 $1x10^{-5}$ s (*vs*. roughly $1x10^{-7}$ s without mass scaling). Simulations of the three-zone axial crush
303 model with and without mass scaling demonstrated no differences, supporting the use of mass
304 scaling in these models.

4. Results

4.1 Three-Point Bend Experiments and Finite Element Model

4.1.1 Quasi-Static Three-Point Bend

Quasi-static three-point bend tests and simulations were conducted for the fully martensitic (QS-3P-FM – see Table 1 for test designations) and tailored soft flange hot stamped conditions (QS-3P-SF). The QS-3P-FM experiments had a consistent peak force, averaging 32.5 kN (Figure 6a), despite having large variability in displacement at failure (28.9 mm to 54.4 mm) due to the specimens exhibiting two distinct failure modes: symmetric failure where the hat section sidewalls deformed uniformly with no out-of-plane rotation (Figure 6b) and asymmetric failure where one sidewall of the hat section deformed (Figure 6c), causing the top hat section to rotate perpendicular to the indenter, delaying failure of the adhesive joint and separation of the flange. The QS-3P-FM model predicted a symmetric failure mode with a peak force of 32.9 kN, in agreement with the experiments (1.2% difference). However, the model predicted a much higher displacement at failure (48 mm) compared to the specimen with symmetric failure (30 mm).

The QS-3P-SF experiments had an average peak force of 23.3 kN, with no large-scale failure of the adhesive joint. A small region of adhesive failure was observed on the inner edge of the flange at both ends of the tube, but this failure did not propagate in a catastrophic manner. The QS-3P-SF finite element model predicted a peak force of 23.4 kN, in agreement with the experiments (0.6% difference). The model also predicted the adhesive damage pattern at the ends of the tubes, as observed in the experiments.

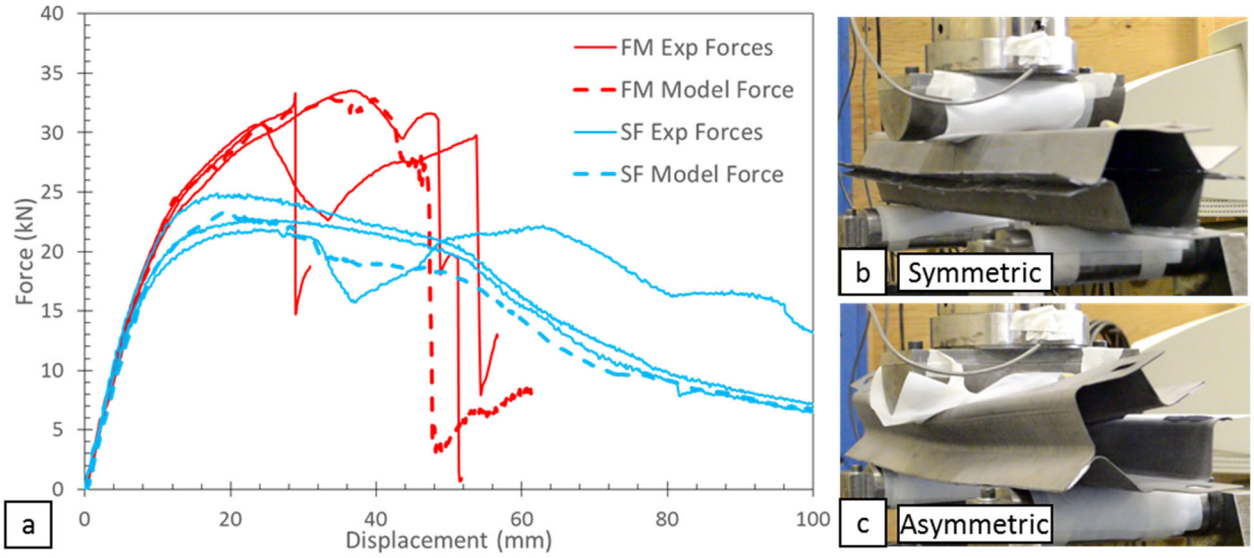

Figure 6: a) Force-displacement response of QS-3P-FM and QS-3P-SF experiments and model predictions, b) example of symmetric deformation, c) example of asymmetric deformation in FM.

4.1.2 Dynamic Three-Point Bend

Dynamic three-point bend tests and simulations were conducted on fully martensitic (DM-3P-FM) and soft flange (DM-3P-SF) structures. The three DM-3P-FM experiments attained an average peak force of 54.7 kN and an average energy absorption of 2.20 kJ at the end of the free crush displacement (55 mm) (Figure 7a). The model had reasonable correlation with the experiments with a predicted peak force of 48.8 kN (10.8% difference) and an energy absorption of 1.85 kJ (15.9% difference). All three experimental specimens exhibited a symmetric failure mode, which was predicted by the model as well (Figure 7b and Figure 7c). However, the model predicted an earlier joint failure and flange separation by up to 22.1% compared to the average of the three tests (50.0 mm).

The three DM-3P-SF experiments had an average peak force of 33.5 kN and an average energy absorption of 1.19 kJ, with no large-scale failure of the adhesive joint. The predicted peak force was in reasonable correlation with the experiments at 28.1 kN (16.0% difference) and the energy absorption was in excellent agreement with the experiments at 1.22 kJ (2.95% difference). A small amount of cohesive failure was observed on the inner edge of the flange at the ends of the tubes. The model was able to accurately capture the gross deformation mode of the tube, and the observed adhesive damage at the ends of the tube.

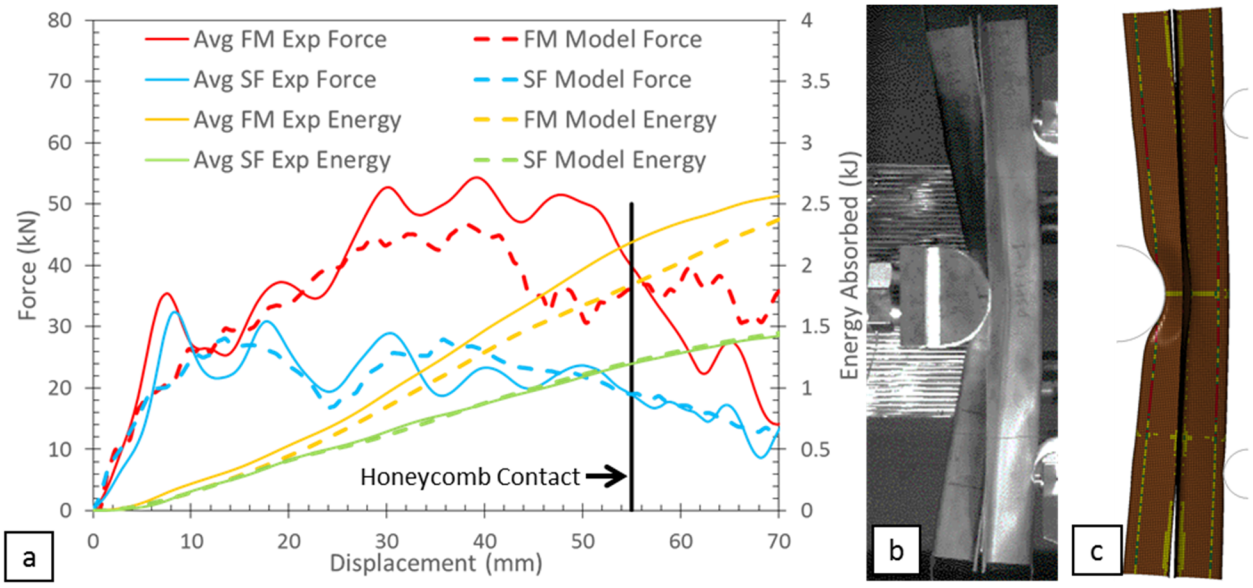

Figure 7: a) Force and energy-displacement responses of DM-3P-FM and DM-3P-SF experiments and model predictions, extent of top hat section deformation at the onset of adhesive failure for b) the DM-3P-FM experiment c) and DM-3P-FM model.

4.2 Axial Crush Experiments and Finite Element Model

4.2.1 Quasi-Static Axial Crush

Quasi-static axial crush tests and simulations were conducted on the fully martensitic (QS-AX-FM) and tailored three zone hot stamped (QS-AX-3Z) structures. The three QS-AX-FM

356 experiments had an average peak force of 260 kN and an average energy absorption of 5.97 kJ at
357 74.0 mm of displacement (Figure 8a). Two of the three experimental specimens failed to trigger
358 a fold at the initiator and exhibited global buckling deformation, in which adhesive joint failure
359 initiated in the middle of the tube and then rapidly propagated along the length of the flange
360 (Figure 8b). Only one of the specimens achieved a local folding deformation that was first
361 triggered by the fold initiator and proceeded to develop a second fold later on, resulting in
362 significantly higher energy absorption compared to the other two tests. The peak force and
363 energy absorption predicted by the finite element model were both in reasonable agreement
364 with the experiments at 300 kN (15.2% difference) and 5.59 kJ (6.31% difference) at 74.0 mm of
365 displacement, respectively. The model also predicted a local folding deformation; however, it
366 initiated in the bottom third of the tube instead of the fold initiator, then gradually transitioned
367 into a global buckling deformation mode instead of developing more folds. The model also
368 predicted a stiffer response compared to the experiments.

369 The three QS-AX-3Z experiments had an average peak force of 148 kN and an average energy
370 absorption of 5.82 kJ at 100 mm of displacement. The tailored property distribution not only
371 promoted all of the specimens to reliably trigger a local folding deformation at the initiator, but
372 also promoted stable continuous folding throughout the test, resulting in a controlled and
373 progressive deformation pattern (Figure 8c). The model predicted a peak force of 168 kN (12.9%
374 difference) and an energy absorption of 6.65 kJ (14.3% difference) at 100 mm of displacement,
375 which were both in reasonable agreement with the experiments. Similar to the QS-AX-FM model,
376 the QS-AX-3Z model predicted a stiffer response compared to the experiments.

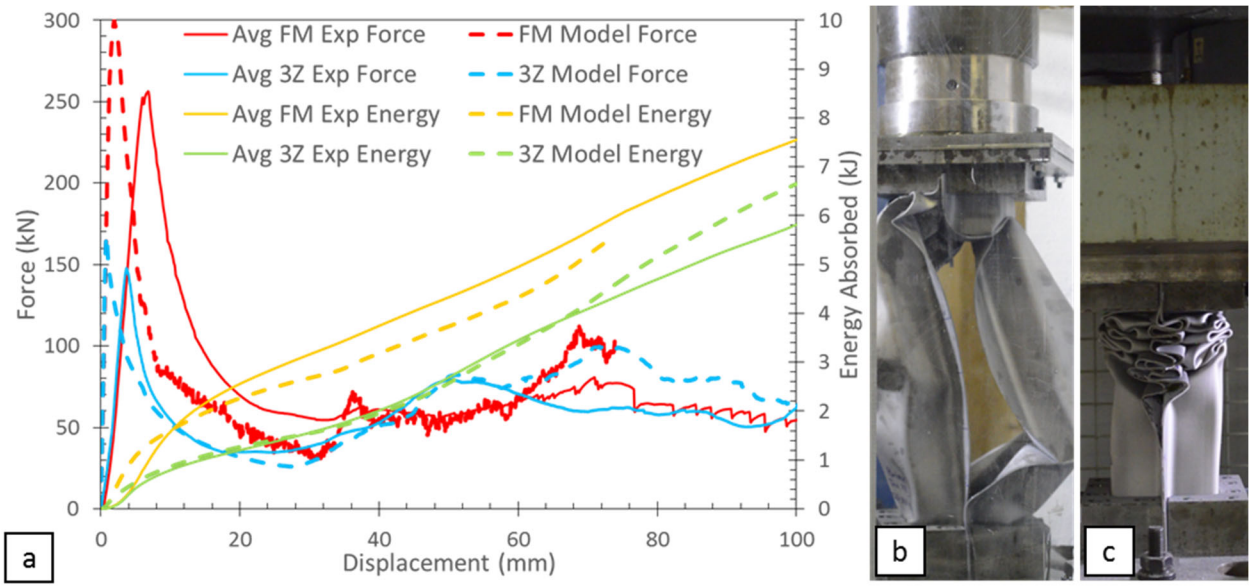

Figure 8: a) Force and energy-displacement responses of QS-AX-FM and QS-AX-3Z experiments and model predictions, b) global buckling of FM tubes and c) progressive folding of 3Z tubes.

4.2.2 Dynamic Axial Crush

Dynamic axial crush tests and simulations were conducted for the fully martensitic (DM-AX-FM) and three zone (DM-AX-3Z) structures. The three DM-AX-FM experiments had an average peak force of 623 kN and an average energy absorption of 14.5 kJ at 145 mm (free crush displacement) (Figure 9a). Contrary to the QS-AX-FM experiments, all three DM-AX-FM specimens exhibited folding deformation beginning at the initiator. After the first fold was triggered, only one of the specimens continued to develop folds past the first one triggered by the initiator, resulting in a controlled deformation pattern. In the other two specimens, adhesive joint failure propagated much faster beyond the active crush zone such that the deformation quickly transitioned into global buckling, resulting in an unstable collapse mode with extensive metal fracture and tearing. The peak force predicted by the model was in reasonable agreement with the experiments at

527 kN (15.4% difference) and the predicted energy absorption was in excellent agreement at 14.2 kJ (2.30% difference). The model did not predict a fold triggering at the initiator. Instead, adhesive failure was initially predicted at the center of the tube, which quickly propagated throughout the rest of the flange, leading to a global buckling deformation.

The DM-AX-3Z experiments had an average peak force of 404 kN and an average energy absorption of 9.77 kJ at 145 mm of crush displacement. The initiator triggered folding deformation that continued throughout the entire impact in a controlled collapse mode (Figure 9b), during which the adhesive joint failure and separation of the flange was limited in extent and did not result in catastrophic joint failure. The three-zone finite element model predicted a controlled collapse mode starting with folding deformation at the initiator that continued throughout the impact simulation (Figure 9c). The peak force predicted by the model agreed with the experiments at 393 kN (2.62% difference), however, the model predicted an energy absorption of 16.3 kJ which was higher (66.9% difference) than the experimental value.

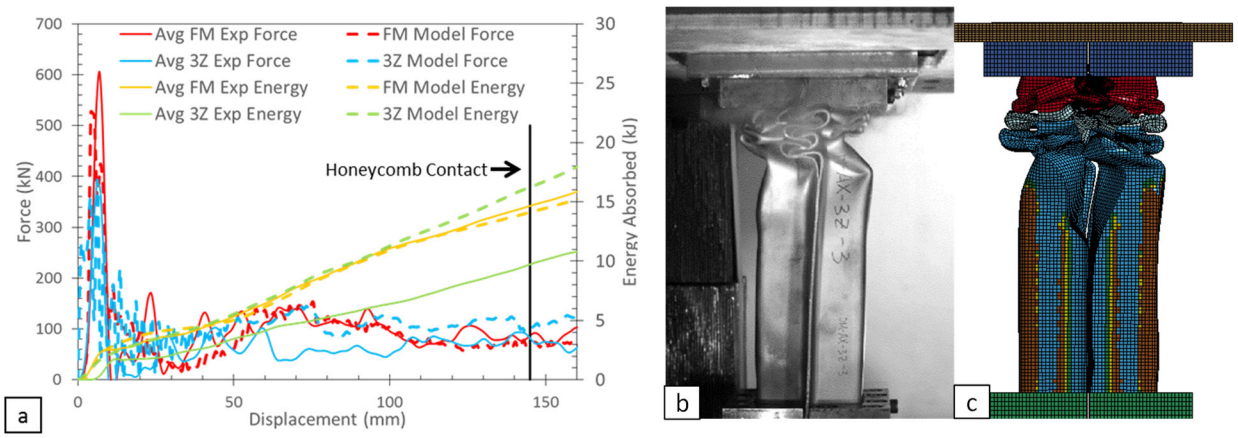

Figure 9: a) Force and energy-displacement response of DM-AX-FM and DM-AX-3Z experiments and model predictions, b) deformation comparison between DM-AX-3Z experiment, c) and model.

4.3 Caiman (Mode I) Experiments and Finite Element Model

Quasi-static Caiman tests and simulations were conducted for fully martensitic (QS-CM-FM) and soft flange (QS-CM-SF) structures. The three QS-CM-FM experiments had an average peak force of 2.97 kN and an average energy absorption of 47.3 J (Figure 10a). Due to the controlled nature of the Caiman experiment (progressive Mode I opening due to peel stress), the QS-CM-FM experiments had a very consistent loading response between all the tests. The predicted peak force and energy absorption from the model were in good agreement with the experiment at 2.89 kN (2.58% difference) and 52.6 J (11.2% difference), respectively. The predicted model response was in excellent agreement with the experiments from the onset of loading to the peak load, where the model then predicted a more gradual unloading compared to the experiment.

The QS-CM-SF experiments had an average peak force of 2.97 kN and an average energy absorption of 60.5 J. The QS-CM-SF experiments had slightly more variability in the loading responses compared to the QS-CM-FM experiments. Both the predicted peak force and energy absorption by the model were in excellent agreement with the experiments at 2.95 kN (0.6% difference) and 64.5 J (6.6% difference), respectively. The QS-CM-SF model predicted a stiffer response as well as a slightly higher rate of adhesive crack propagation (force unloading) compared to the QS-CM-SF experiments.

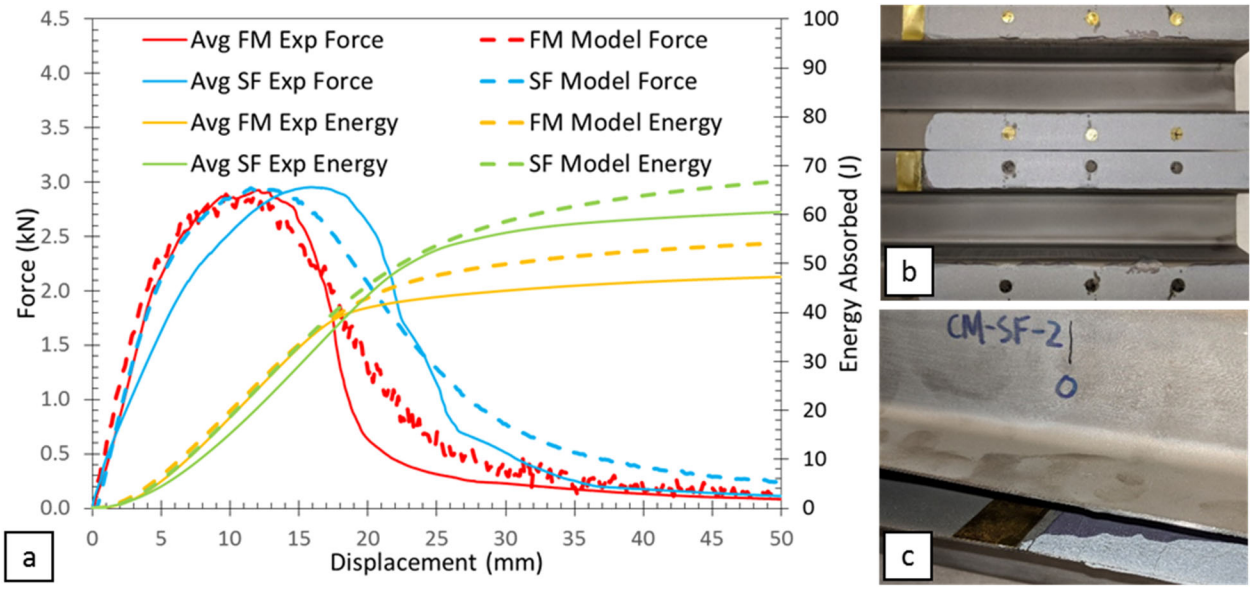

Figure 10: a) Force and energy-displacement responses of QS-CM-FM and QS-CM-SF experiments and model predictions, b) failure surface of FM flanges, and c) and failure surface of the SF.

The Caiman experiments produced very consistent results for the model to be assessed against, and the model predictions were in excellent agreement with the experiments. In addition to the global metrics such as the shape of the force-displacement response, peak force, and energy absorption, a local metric was used to more directly assess the ability of the CZM adhesive model to predict the joint behavior. The first local metric investigated was crack advance, which compared the crack propagation (change in length of the cracked adhesive along the length of the flange) to the loading pin displacement measured by the load frame. Using the synchronized test video, the position of the crack front was optically tracked and converted to a displacement (Figure 11a), using the length of the bond line as a calibration measurement. The FM experiments demonstrated very consistent results over three tests (Figure 11b), though the FM model predicted an onset of crack propagation at a load point displacement that was roughly 2 mm

earlier. The rate of crack propagation immediately after the initiation in the model was also observed to be lower than that of the FM specimens, until the rates converged at roughly 26 mm of pin displacement. Similarly, the SF model predicted an early onset of crack propagation by roughly 4 mm (same pin displacement of 14 mm as the FM model) with a lower initial rate of propagation. Additionally, the SF test response exhibited cycles of slow and rapid propagation rate, resulting in a step-wise pattern in the crack advance response that was not captured by the model.

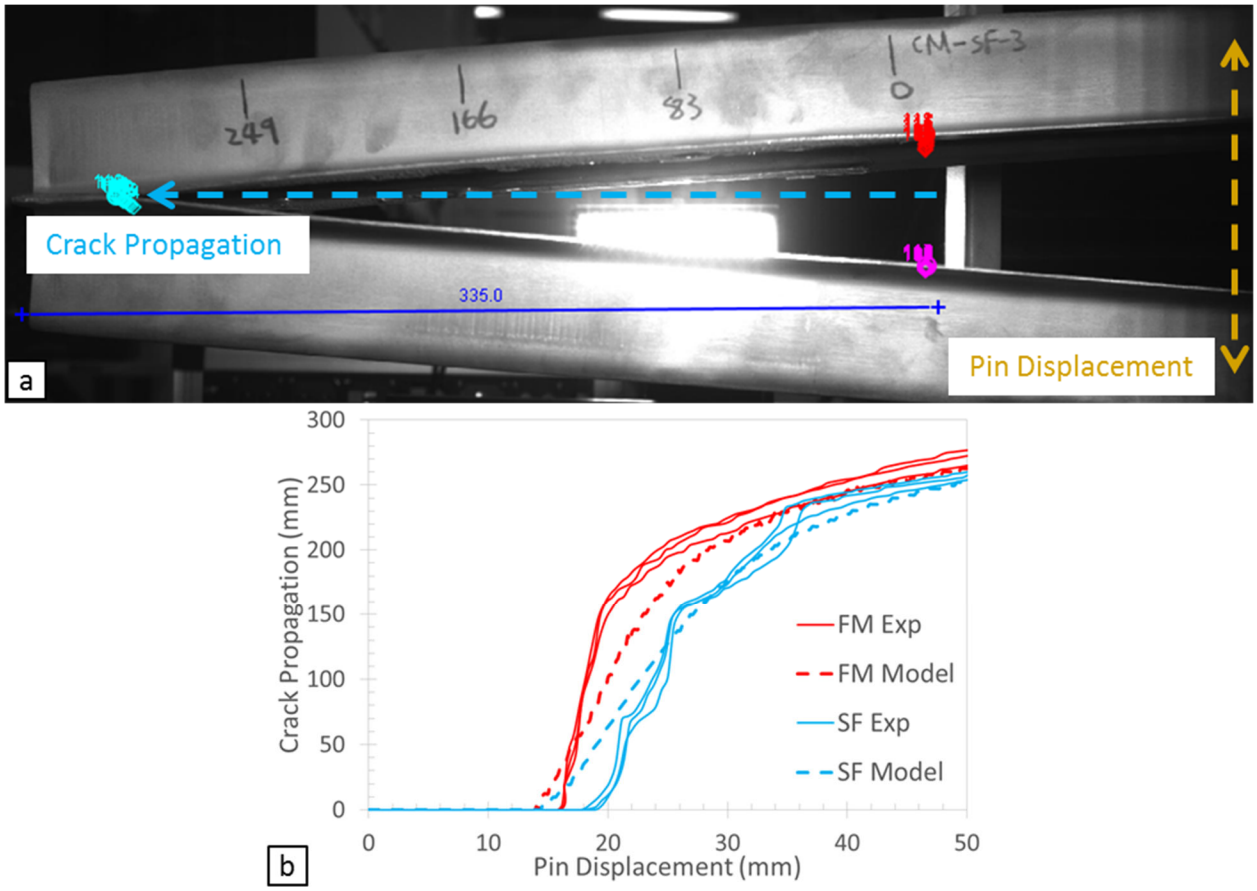

Figure 11: a) Tracking the flange opening in the Caiman experiment, and b) plot of crack extension. the crack advance plot (b)

5. Discussion

The finite element models provided a good representation of both the fully martensitic and soft flange structures under three-point bending loading, for the experiments that exhibited symmetric deformation. Differences in response occurred primarily for the martensitic tubes that could demonstrate asymmetric deformation in some cases, attributed to small differences in alignment or initial specimen geometry. Although the predicted peak force in the QS-3P models was in good agreement with the experiments, the quasi-static model over predicted the failure displacement and the dynamic model under predicted this response. The limited ability of the model to accurately predict three-point bend failure displacement in this work may be attributable to the geometric instability caused by the 1.2 mm material thickness. The intent of three-point bending was to produce Mode II loading (shear) in the adhesive joint along the neutral axis. However, localized deformation of the top hat section, as opposed to bending of the entire tube structure, resulted in mixed-mode loading on the adhesive joint. One possible way to impose more Mode II loading in future work would be to place rigid inserts into the tube to support the top hat section to minimize its local deformation.

The loading responses predicted by the axial crush models were stiffer than the experiments for both the QS-AX-FM and QS-AX-3Z cases. This could be attributed to the compliance in the test setup, including the fixtures and load frame, compared to the rigid boundary conditions in the model. Besides this observed difference in stiffness, the loading response of the axial crush experiments was generally very consistent and the models were in reasonable agreement with the experiments, for both the FM and 3Z conditions. The FM experiments were much less repeatable due to these specimens being much more likely to globally buckle than to successfully

trigger progressive folding at the initiator. The FM models for both quasi-static and dynamic loading rates did not predict a fold at the initiator and generally resulted in global buckling deformation as well with an unstable collapse mode and extensive metal fracture. On the other hand, the 3Z tailoring resulted in the desired fold initiation, which lead to consistent deformation patterns with a progressive and controlled collapse mode that was well captured by the modified 3Z model.

The Caiman specimen geometry provided controlled loading with a lesser dependence on the structural response compared to the three-point bend and axial crush specimens, providing a more direct assessment of the adhesive and corresponding adhesive model. Use of the Caiman specimen geometry allowed for the assessment of a vehicle structure-level component, including the forming history and surface morphology, enabling understanding of performance in vehicle structures. The effect of SF tailoring on the Caiman specimens could be observed in the crack advance behavior. The step-wise pattern in the crack advance response of SF Caiman specimens was likely due to energy absorbed by the more ductile flanges through plastic deformation.

When comparing the response of the martensitic versus tailored structures, in general the high strength of the martensitic structures placed higher loads on the adhesive joint and the lack of plastic deformation in the steel channel led to more rapid crack propagation in the adhesive, and generally more variable response in the experimental failure modes. For example, the martensitic axial crush tubes did not demonstrate consistent initiation of folding, or progressive folding and energy absorption, while the three-zone specimens did achieve controlled deformation. For adhesive only joints, the current study demonstrated that consistent structural response also correlated with improved model predictions; whereas less controlled modes (e.g. out-of-plane

deformation in three-point bending, or initiation of folding away from the initiator in axial crush) resulted in higher variability in predicting the adhesive joint response.

One aspect of tailoring that was not considered in the numerical models was warpage of the hat sections resulting from the hot stamping process. Both the SF and 3Z tailoring introduced bowing along the length of the final parts. As a result, the bonding process introduced some residual stresses in the adhesive joint that were not considered in the current models and should be investigated in future work.

While the current work used adhesive-only joints for the purpose of model validation, future work should investigate the effect of hybrid joints combining adhesives with welds or mechanical fasteners and how they potentially augment the performance of adhesives.

6. Conclusions

The current study investigated the fidelity of a CZM structural adhesive model for automotive-scale structures created by adhesively joining two formed hat-sections with different hot stamping processes and three modes of loading. The conclusions stemming from this work are as follows:

- Structural adhesive (IRSA 07333, 3M) can be used to join tailor hot stamped ultra-high strength steel to achieve consistent loading response and crack advance characteristics, provided that proper steps for surface preparation are performed.
- The shimming and surface preparation technique developed to bond structures enabled uniform adhesive coverage and consistent bond line thickness throughout the flange. This technique could potentially be adapted to hybrid joints involving mechanical fasteners and adhesives.
- With the bonding procedure developed in this study, it was demonstrated that adhesively bonded tailored hot stamped UHSS tubes could achieve a consistent loading response under various load conditions and rates. Tailoring of the UHSS also contributed to minimizing the likelihood of rapid debonding of the adhesive joint, thereby preventing a global buckling deformation and unstable collapse modes.
- The effect of tailoring hot stamped components allowed some of the energy to be dissipated through plastic deformation of the parent metal. For axial crush specimens, tailoring led to desired fold initiation that continued to stabilize the collapse of the tube.

For Caiman specimens, tailoring led to a delay in the onset of crack propagation and also subsequent propagation rate with an increase in energy absorption.

- The Caiman experiment has been shown to be valuable when applied to full scale adhesive structural testing, as it provided a progressive and controlled crack propagation behavior that was useful as validation data for the CZM adhesive model.
- Overall, the predicted global loading response correlated well with the measured response for all experiments in the initial load up to peak force. With a few exceptions, the CZM adhesive model was able to predict the peak force, displacement-to-failure, and energy absorption within 16% of the measured values.

Acknowledgements

The authors would like to express thanks to Honda Development & Manufacturing of America, 3M Canada Company, ArcelorMittal, Ontario Centers of Excellence, the Ontario Advanced Manufacturing Consortium, Compute Canada and the Natural Sciences and Engineering Research Council of Canada (NSERC) for their support of this research. This research was undertaken, in part, thanks to funding from the Canada Research Chairs Program.

References

[1] Goede, M (2009). Sustainable Production Technologies of Emission Reduced Lightweight Car Concepts (Superlight-Car): Publishable Final Activity Report; *European Commission Community Reshearch and Development Information Service: Brussles*

[2] Conklin, J, Beals, R, Brown, Z (2015) BIW Design and CAE. *SAE Tech. Pap. Ser.2015*, 2015-01-0408. DOI: 10.4271/2015-01-0408.

[3] Symietz, D (2005). Structural Adhesive Bonding: The Most Innovative Joining Technique for Modern Lightweight Design, Safety and Modular Concepts -Progress Report-. SAE International.

[4] Marzi, S, Hesebeck, O, Brede, M, & Kleiner, F (2009). A Rate-Dependent Cohesive Zone Model for Adhesively Bonded Joints Loaded in Mode I A Rate-Dependent Cohesive Zone Model for Adhesively. Journal of Adhesion Science and Technology, 23(6), 881–898. https://doi.org/10.1163/156856109X411238

[5] Goglio, L, Peroni, L, Peroni, M, Rossetto, M (2008). High strain-rate compression and tension behaviour of an epoxy bi-component adhesive. Int J Adhes Adhes 28:329–339

[6] George, R, Bardelcik, A, & Worswick, MJ (2012). Hot forming of boron steels using heated and cooled tooling for tailored properties. Journal of Materials Processing Technology, 212(11), 2386–2399. https://doi.org/10.1016/j.jmatprotec.2012.06.028

[7] Mori, K, Bariani, PF, Behrens, BA, Brosius, A, Bruschi, S, Maeno, T, … Yanagimoto, J (2017). Hot Stamping of Ultra-High Strength Steel Parts. CIRP Annals - Manufacturing Technology, 66(2), 755–777. https://doi.org/10.1016/j.cirp.2017.05.007

[8] Bardelcik, A, Worswick, MJ, Wells, Ma (2014). The Influence of Martensite, Bainite and Ferrite on the As-Quenched Constitutive Response of Simultaneously Quenched and Deformed Boron Steel - Experiments and Model. Materials and Design, 55, 509–25. doi: 10.1016/j.matdes.2013.10.014

[9] Karbasian, H, Tekkaya, AE (2010). A Review on Hot Stamping. Journal of Material Processing Technology, 210, 2103–18. doi: 10.1016/j.jmatprotec.2010.07.019.

[10] Merklein, M, Wieland, M, Lechner, M, Bruschi, S, & Ghiotti, A (2016). Hot stamping of boron steel sheets with tailored properties: A review. Journal of Materials Processing Technology, 228, 11–24. https://doi.org/10.1016/j.jmatprotec.2015.09.023

[11] Eller, TK, Greve, L, Andres, MT, Medricky, M, Hatscher, A, Meinders, VT, & Van Den Boogaard, AH (2014). Plasticity and fracture modeling of quench-hardenable boron steel with tailored properties. Journal of Materials Processing Technology, 214(6), 1211–1227. https://doi.org/10.1016/j.jmatprotec.2013.12.015

[12] Prajogo, Y (2015). Hot Stamping of a Boron Steel Side Impact Beam with Tailored Flange Properties. MASc. University of Waterloo

[13] Omer, K, ten Kortenaar, L, Butcher, C, Worswick, M, Malcolm, S, & Detwiler, D (2017). Testing of a hot stamped axial crush member with tailored properties – Experiments and models. International Journal of Impact Engineering, 103, 12–28. https://doi.org/10.1016/j.ijimpeng.2017.01.003

[14] Tolton, C., O'Keeffe, C., Mohammadizadeh, A., Imbert. J., Worswick, M., Investigation of Resistance Spot Weld Failure in Tailor Hot Stamped Assemblies, International Journal of Impact Engineering, 180, 104677, https://doi.org/10.1016/j.ijimpeng.2023.104677, 2023.

590 [15] Fay PA, Suthurst GD (1990) Redesign of adhesively bonded box beam sections for
591 improved impact performance. Int J Adhes Adhes 10:128–138
592 [16] Belingardi G, Goglio L, Rossetto M (2005) Impact behaviour of bonded built-up beams:
593 experimental results. Int J Adhes Adhes 25:173–180
594 [17] Yang, X, Xia, Y, Zhou, Q, Wang, PC, & Wang, K (2012). Modeling of high strength steel
595 joints bonded with toughened adhesive for vehicle crash simulations. International
596 Journal of Adhesion and Adhesives, 39, 21–32.
597 https://doi.org/10.1016/j.ijadhadh.2012.06.007
598 [18] May, M, Hesebeck, O, Marzi, S, Böhme, W, Lienhard, J, Kilchert, S, Brede, M & Hiermaier,
599 S (2015). Rate Dependent Behavior of Crash-Optimized Adhesives–Experimental
600 Characterization, Model Development, and Simulation. Engineering Fracture Mechanics,
601 133, 112-137. https://doi.org/10.1016/j.engfracmech.2014.11.006
602 [19] Deb, A, Chou, CC, Srinivas, GR, Gowda, S, & Kurnool, G (2016). Behavior of Adhesively
603 Bonded Steel Double Hat-Section Components under Axial Quasi-Static and Impact
604 Loading. SAE 2016 World Congress and Exhibition, 2016–April(April).
605 https://doi.org/10.4271/2016-01-0395
606 [20] Gowda, S, Deb, A, Kurnool, G, & Chou, CC (2018). Behavior of Adhesively Bonded Steel
607 Double-Hat Section Components under Lateral Impact Loading. SAE Technical Papers,
608 2018–April, 1–8. https://doi.org/10.4271/2018-01-1447
609 [21] Lee, MH, Kim, HY, & Oh, SI (2006). Crushing test of double hat-shaped members of
610 dissimilar materials with adhesively bonded and self-piercing riveted joining methods.
611 Thin-Walled Structures, 44(4), 381–386. https://doi.org/10.1016/j.tws.2006.04.012

612 [22] Peroni, L, Avalle, M, & Belingardi, G (2009). Comparison of the energy absorption
613 capability of crash boxes assembled by spot-weld and continuous joining techniques.
614 International Journal of Impact Engineering, 36(3), 498–511.
615 https://doi.org/10.1016/j.ijimpeng.2008.06.004
616 [23] Avalle, M, Peroni, L, Peroni, M, & Scattina, A (2010). Bi-Material Joining for Car Body
617 Structures: Experimental and Numerical Analysis Bi-Material Joining for Car Body
618 Structures: The Journal of Adhesion, 86(5–6), 539–560.
619 https://doi.org/10.1080/00218464.2010.484308
620 [24] Trimiño, LF, & Cronin, DS (2014). Non-Direct Similitude Technique Applied to the Dynamic
621 Axial Impact of Bonded Crush Tubes. International Journal of Impact Engineering, 64, 39–
622 52. https://doi.org/10.1016/j.ijimpeng.2013.10.001
623 [25] da Silva, LFM, & Campilho, RDSG (2012). Advances in numerical modelling of adhesive
624 joints. SpringerBriefs in Applied Sciences and Technology.
625 [26] Trimiño, LF, & Cronin, DS (2016). Evaluation of Numerical Methods to Model Structural
626 Adhesive Response and Failure in Tension and Shear Loading. Journal of Dynamic
627 Behavior of Materials, 2(1), 122–137. https://doi.org/10.1007/s40870-016-0045-7
628 [27] Ji, G, Ouyang, Z, Li, G, Ibekwe, S, Pang, SS (2010). Effects of Adhesive Thickness on Global
629 and Local Mode-I Interfacial Fracture of Bonded Joints. International Journal of Solids
630 Structures. 47, 2445–2458
631 [28] Yang, QD, Thouless, MD (2001). Mixed-Mode Fracture Analyses of Plastically-Deforming
632 Adhesive Joints. International Journal of Fracture, 110(2), 175–187. DOI:
633 10.1023/A:1010869706996.

[29] Campilho, RDSG, Banea, MD, Neto, JABP, & Da Silva, LFM (2013). Modelling Adhesive Joints with Cohesive Zone Models: Effect of the Cohesive Law Shape of the Adhesive Layer. International Journal of Adhesion and Adhesives, 44, 48–56. https://doi.org/10.1016/j.ijadhadh.2013.02.006

[30] Watson, B, Liao, CH, Worswick, MJ, & Cronin, DS (2020). Mode I traction-separation measured using rigid double cantilever beam applied to structural adhesive. *The Journal of Adhesion*, 96(8), 717-737. https://doi.org/10.1080/00218464.2018.1502666

[31] Liao, CH, Watson B, Worswick, MJ, Cronin, DS (2017). 'Mode I Rigid Double Cantilever Beam Test and Analysis Applied to Structural Adhesives.' Dynamic Behavior of Materials, Volume 1, Conference Proceedings of the Society for Experimental Mechanics Series, pp.73-81

[32] Elmer's Products Inc. (2015). Krazy Glue Safety Data Sheet. Viewed 9 May 2019, <http://www.krazyglue.com/docs/default-source/MSDS-Sheets/skg0583.pdf?sfvrsn=8>

[33] Bardelcik, A, Worswick, MJ, Winkler, S, Wells, MA (2012). A Strain Rate Sensitive Constitutive Model for Quenched Boron Steel with Tailored Properties. International Journal of Impact Engineering, 50, 49–62. doi: 10.1016/j.ijimpeng.2012.06.007

[34] ten Kortenaar, L (2016). Failure Characterization of Hot Formed Boron Steels with Tailored Mechanical Properties. MASc. University of Waterloo

[35] Tummers, M., Omer, K., Abedini, A., Peister, C., Butcher, C., Worswick, M. J., … Soldaat, R. (2018). Introduction of a 1000 MPa crush tip within a Usibor® 1500-AS axial crush rail using in-die heated hot stamping. IOP Conference Series: Materials Science and Engineering, 418(1). https://doi.org/10.1088/1757-899X/418/1/012126

[36] Samadian, P, ten Kortenaar, L, Omer, K, Butcher, C, Worswick, MJ (2020). Fracture characterization of tailored Usibor® 1500-AS and damage modelling based on a coupled-micromechanical-phenomenological strategy. Engineering Fracture Mechanics, 223, 106785. https://doi.org/10.1016/j.engfracmech.2019.106785

[37] Watson, B, Worswick, MJ, & Cronin, DS (2020b). Quantification of Mixed Mode Loading and Bond Line Thickness on Adhesive Joint Strength Using Novel Test Specimen Geometry. The International Journal of Adhesion and Adhesives. https://doi.org/10.1016/j.ijadhadh.2020.102682

[38] Watson, B, Nandwani, Y, Worswick, MJ, & Cronin, DS (2019). Metallic Multi-Material Adhesive Joint Testing and Modeling for Vehicle Lightweighting. International Journal of Adhesion and Adhesives, 95, 102421. https://doi.org/10.1016/j.ijadhadh.2019.102421

[39] Seattle Safety, "Decelerator Sled Systems," [Online]. Available: http://www.seattlesafety.com/wp-content/uploads/2014/03/Decel_brochure_10.06.pdf. [Accessed 17 Oct 2020]